On the Denaturation Mechanisms of the Ligand Binding Domain of Thyroid Hormone Receptors

Leandro Martínez,[†] Paulo C. T. Souza,[†] Wanius Garcia,[‡] Fernanda A. H. Batista,[‡] Rodrigo V. Portugal,[‡] Alessandro S. Nascimento,[‡] Marcel Nakahira,[‡] Luis M. T. R. Lima,[§] Igor Polikarpov,[‡] and Munir S. Skaf*,[†]

Institute of Chemistry, State University of Campinas-UNICAMP, P.O. Box 6154, Campinas, SP, 13084-862, Brazil, Instituto de Física de São Carlos, Universidade de São Paulo, Av. Trabalhador SaoCarlense 400-IFSC-Grupo de Crystalografia, P.O. Box 369, Sao Carlos, SP, 13560-970, Brazil, and Faculdade de Farmácia, Universidade Federal do Rio de Janeiro, CCS, bloco B, subsolo, sala 34. Ilha do Fundão, Rio de Janeiro, RJ, 21941-590, Brazil

Received: December 5, 2009

The ligand binding domain (LBD) of nuclear hormone receptors adopts a very compact, mostly α-helical structure that binds specific ligands with very high affinity. We use circular dichroism spectroscopy and high-temperature molecular dynamics simulations to investigate unfolding of the LBDs of thyroid hormone receptors (TRs). A molecular description of the denaturation mechanisms is obtained by molecular dynamics simulations of the TRα and TRβ LBDs in the absence and in the presence of the natural ligand Triac. The simulations show that the thermal unfolding of the LBD starts with the loss of native contacts and secondary structure elements, while the structure remains essentially compact, resembling a molten globule state. This differs from most protein denaturation simulations reported to date and suggests that the folding mechanism may start with the hydrophobic collapse of the TR LBDs. Our results reveal that the stabilities of the LBDs of the TRα and TRβ subtypes are affected to different degrees by the binding of the isoform selective ligand Triac and that ligand binding confers protection against thermal denaturation and unfolding in a subtype specific manner. Our simulations indicate two mechanisms by which the ligand stabilizes the LBD: (1) by enhancing the interactions between H8 and H11, and the interaction of the region between H1 and the Ω-loop with the core of the LBD, and (2) by shielding the hydrophobic H6 from hydration.

1. Introduction

Nuclear hormone receptors (NRs) are the largest family of transcription factors of eukaryotes.[1−3] NRs are one of the most prominent targets for pharmaceutical development because of their broad spectrum of functionality in humans. Steroids, vitamins A and D, thyroid hormones, and contraceptives are just a few examples of pharmaceuticals that act by binding and activating nuclear hormone receptors.[4] NRs such as the retinoic acid receptor (RAR), the thyroid hormone receptor (TR), and the receptors of sexual hormones progesterone, testosterone, and estrogen have important roles on tissue development and differentiation, and are involved in several types of human cancers.[5]

Nuclear receptors are proteins of variable size containing three domains: An N-terminal domain, a DNA binding domain (DBD), and a ligand binding domain (LBD). The structure of the N-terminal domain is mostly unknown and appears to be unstructured in solution. The DBD and the LBD, on the other hand, have well-known folds.[6] The DBD folds into a double zinc-finger motif responsible for binding specific response elements in the DNA, whereas the LBDs are very compact, mostly α-helical structures, composed of about 12 helices and a few β strands. The ligand binding pocket is buried in the hydrophobic core of the domain.[7−17] Similar to other NRs, TRs interact with specific hormone response elements within target promoters via their DBDs. The TRs then utilize multiple protein−protein interaction surfaces to assemble the active transcription heterodimer complexes with retinoid X receptors (RXRs) and coactivator/corepressor complexes that, in turn, modify gene expression by remodeling local chromatin and recruiting the transcription machinery.

Most of what is known about the structure and function of nuclear receptors at a molecular level has been obtained from crystallographic analyses which, in spite of the wealth of atomic details, provide limited dynamical information. This poses several questions of biological relevance: How does the mobility of the LBD affect ligand binding affinity? How do ligands bind to and dissociate from these receptors? Which are the mechanisms of thermal denaturation of nuclear receptors? How do ligands affect such processes? How does the LBD fold? As new structural models of NR LBDs become available, answers to these questions are being unveiled with experimental and theoretical methods.[18−26]

The description of the denaturation mechanisms of any protein is very challenging. Detection of molecular mechanisms and intermediate states is not always accessible experimentally. In addition, the unfolding rates of stable proteins are rarely below the microsecond range, even under severe conditions of high temperatures and high concentration of denaturant species. Such processes are too slow for realistic computer simulations.[27] From the computational point of view, the study of the denaturation of NRs LBDs poses still a greater challenge, since their very

* To whom correspondence should be addressed. E-mail: skaf@iqm.unicamp.br.
[†] State University of Campinas.
[‡] Universidade de São Paulo.
[§] Universidade Federal do Rio de Janeiro.

10.1021/jp911554p
Published on Web 12/31/2009

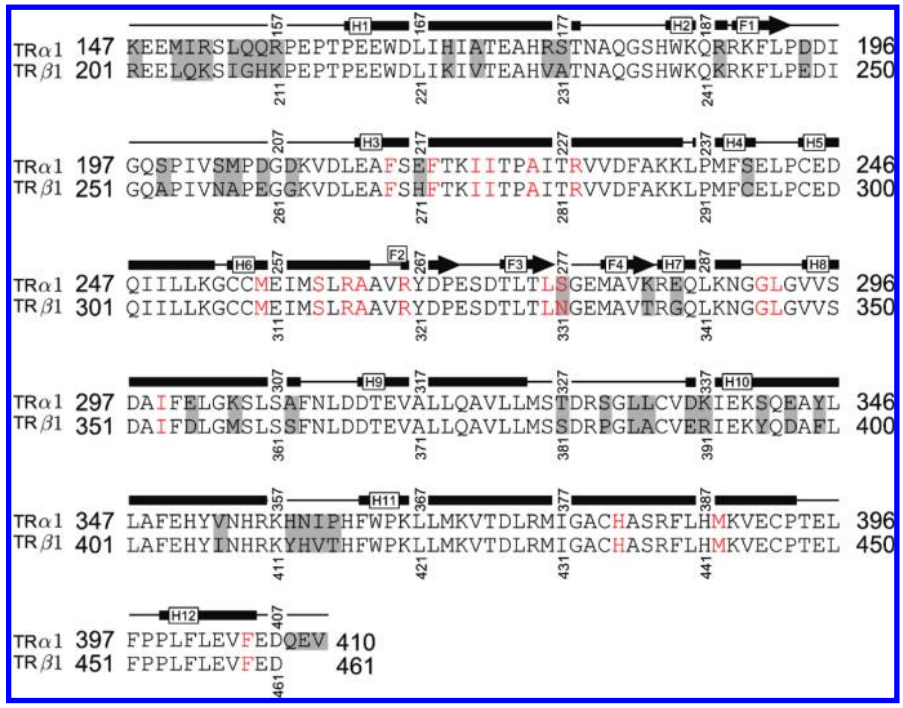

Figure 1. Sequence and canonical secondary structure of the LBDs of hTRα and hTRβ. Residues that differ in both isoforms are shaded, and residues belonging to the binding site are in red.

compact folds are stable even at temperatures well above the physiological ones.

Simulations of protein denaturation have suggested that proteins start to unfold by the expansion of their hydrophobic cores. This expansion leads the identifiable transition state, which has relatively small structural deviations from the native structure.[28] Simulations starting from these structures at physiological temperatures restore the native fold, while simulations starting after the transition state evolve to denatured or partially denatured structures.[28,29] Nevertheless, the exact sequence of events of folding or unfolding seems to be protein-dependent. For example, Zhou and Karplus proposed that during folding of a small α-helical protein, intrahelical contacts can be formed rapidly in the absence of collapse.[30] For other proteins, however, it has been experimentally observed that the hydrophobic collapse precedes formation of the secondary structure.[31] Virtually all these studies have focused on the denaturation of peptides, small proteins (usually less than 150 residues), or proteins known to have fast folding kinetics.[28] In this work we provide the first molecular picture of the denaturation mechanisms of the LBD of a nuclear receptor and investigate how they are affected by ligand binding.

Insights into the denaturation of the NR LBDs are interesting since these domains are relatively large, composed of about 260 residues, and differ from reported protein denaturation simulations in two very important aspects: First, there are structural motifs within the LBD structure (whole α-helices, for example) that are completely buried within the protein core and have no contact with the solvent in the native state. Proteins such as barnase,[32] BPTI,[33] the engrailed homeodomain,[27] and the villin headpiece subdomain,[34] among others,[28,35,36] for which the denaturation mechanisms have been studied by computer simulations, do not exhibit complete elements of the secondary structure protected from solvent. Moreover, knowledge of the denaturation pathways of the LBDs may help to identify residues that are important for large-amplitude motions of the protein and, therefore, contributes to better understanding the molecular basis of the diseases caused by their mutations. Second, the vast majority of available computational studies on protein denaturation were performed on proteins that do not bind ligands. In this work we show experimentally that the ligand plays an important role in TRs stabilization and use MD simulations to investigate the underlying molecular reasons. Moreover, the denaturation mechanisms suggested by the simulations provide insights into the folding pathways of this important protein family. The mechanisms proposed may be general for other NRs.

Here we focus on the denaturation of two isoforms of the human thyroid hormone receptor, hTRα and hTRβ (hereafter referred simply as TRα and TRβ). A sequence alignment of the two subtypes is shown in Figure 1. TRs are important for the regulation of the basal metabolism, for the control of serum cholesterol levels, and for tissue differentiation.[5] TRs are related to important human diseases such as cancer, obesity, hypothyroidism and hyperthyroidism, and the thyroid hormone resistance syndrome. The TRα subtype is found mostly in heart tissues and plays an important role in the control of cardiac activity. TRβ is predominantly expressed in the liver and is responsible for fat loss and control of metabolic rates. Some of the ligands that bind TRβ selectively have a very promising pharmaceutical potential since they increase the metabolic rate and lower cholesterol levels without promoting deleterious effects on heart tissues.[5,9,13] Although these effects were already demonstrated in vivo and several TRβ selective ligands have been developed, there is so far no such drug approved for human administration.[37]

In this work we present results from molecular dynamics simulations of denaturation of TR LBDs which suggest a mechanistic picture of the denaturation process. We also report results from circular dichroism experiments (far-UV CD) on the thermal denaturation of the LBDs of TRα and TRβ bound to the natural β-selective ligand Triac (a comprehensive analysis of Triac binding and selectivity, and additional thermal denaturation experiments with Triac and other ligands are described in Martínez et al.[26]). Our experimental data show that the

denaturation mechanism of the TR-LBD is highly dependent on ligand binding and to different extents for each subtype. High temperature simulations suggest that denaturation of TR-LBD proceeds through the loss of native contacts and secondary structure prior to the expansion of the hydrophobic core, contrary to smaller proteins that tend to lose the compactness of their hydrophobic core before rupturing of secondary structural features.[28](b) Details of the denaturation mechanisms are provided. Ligand-induced stabilization and folding mechanisms are discussed in view of the simulation results.

2. Materials and Methods

A. Ligand-Induced Thermal Stability and Protein Denaturation. The human-TRβ ligand binding domain (TRβ LBD) region encompassing residues 202−461 and the human-TRα (TRα) LBD covering residues 148−410 were expressed in *E. coli* and purified as described previously,[14,38] and their purities were checked by SDS-PAGE. Thermal unfolding of TRα and TRβ LBDs were monitored by far-UV CD spectroscopy, over a wavelength range of 200−250 nm, using a J-715 Jasco spectropolarimeter equipped with a temperature control. CD spectra were measured from samples in 1 mm path length quartz cuvettes and were the average of 16 accumulations, using a scanning speed of 100 nm/min, a spectral bandwidth of 1 nm, and a response time of 0.5 s. The TRα and TRβ LBDs concentrations were 5 μM in 20 mM phosphate (pH 7.4) buffer, 50 mM NaCl, 1 mM DTT, 5% glycerol in the presence or absence of Triac (15 μM). All spectra were smoothed by Fourier filtering prior to subsequent analysis. Thermal denaturation of TRα and TRβ LBDs were characterized by measuring the ellipticity changes[39] at 222 nm induced by a temperature increase from 293 to 363 K at steps of 2 deg. Subsequently, 16 data acquisition scans were recorded, each of which took 30 s, leading to a total of 12 min per data point. CD spectra were obtained on a degree ellipticity scale. The buffer contribution was subtracted in all of the experiments. The fraction of denatured protein (α) was calculated from the ellipticities by $\alpha = (\theta_{folded} - \theta_{obs})/(\theta_{folded} - \theta_{unfolded})$, where θ_{obs} is the ellipticity at a particular temperature and θ_{folded} and $\theta_{unfolded}$ are the values of the ellipticity characteristic of the denatured and native states, respectively. To determine the apparent T_m and enthalpy of folding, data were fit to the following equations, assuming that all the ellipticity change was due to a two-state transition between the folded and unfolded receptor: $k = \exp\{[\Delta H/(RT)][(T/T_m) - 1]\}$, $\alpha = k/(1 + k)$, where ΔH is the apparent van't Hoff enthalpy of folding, T_m is the midpoint of the folding transition (melting temperature), and R is the ideal gas constant.

B. Molecular Dynamics Simulations. The structures of TRα and TRβ bound to Triac were recently obtained by our research group and were refined to 2.0 and 2.5 Å, respectively.[26] The complete simulated systems were built with Packmol,[40,41] containing the LBD of either subtype, water, and one counterion for each charged residue for electroneutrality: 43 Na^+ and 30 Cl^- ions for TRα and 43 Na^+ and 30 Cl^- for TRβ bound to Triac. For the apo-structures of both LBD subtypes there is one less Na^+ in solution. We use a cubic box with 16600 waters molecules with side dimensions of 81 Å for the constant-temperature simulations. The average thickness of the hydration layer is approximately 25 Å. Auxiliary simulations in which the temperature was gradually increased (see below) were performed using larger cubic boxes (86 Å), containing 18000 water molecules, because greater levels of protein denaturation and expansion are reached during these runs. In all cases, the box dimensions were chosen such that the solvent density away from the protein surface equals that of ambient water (1 g/cm^3). Therefore, above 298 K, the systems are pressurized. The average pressure of the 498 K simulations described below was approximately 4.2 kbar. Similar conditions have been used for studying thermal denaturation of proteins using high temperature MD simulations.[27−36]

All simulations were performed with NAMD[42] applying periodic boundary conditions and CHARMM parameters.[43] The TIP3P model was used for water.[44] The parameters for the ligands were reported previously.[20,21] A time-step of 2.0 fs was used in the control and constant temperature simulations. For the increasing temperature denaturation runs the time step was 1.5 fs. All hydrogen-to-heavy-atom bonds were kept rigid. A 14 Å cutoff with smooth switching function starting at 12 Å was used for the van der Waals interactions, whereas electrostatic forces were treated via the particle mesh Ewald method.[45]

Equilibration was performed as follows: The energy of the system was minimized by 700 conjugate gradient (CG) steps keeping all protein atoms fixed, except the modeled regions, which were always allowed to move. Fixing only the Cα atoms, another 500 CG steps were performed. Finally 300 CG steps were carried out without any restrictions. After minimization, 2 ns MD simulations were performed under constant temperature and pressure conditions (NPT) at 298 K, with velocity rescaling every 2 ps and Langevin barostat with damping coefficient of 5 ps^{-1}. Three independent control simulations of the TRα and TRβ LBDs bound to Triac and also ligand-free were performed in the NPT ensemble at 298 K and 1 bar under similar conditions, lasting 20 ns each. The control simulations reproduce relatively well the mobility of the LBD, as inferred from temperature B-factors from crystallographic structures (Figure 2), thus providing additional validation of the MD simulation protocols. A total of nine independent 20 ns simulations were carried out at 498 K for the holo- and apo-structures of both LBD subtypes for the denaturation analyses under NVT conditions. The initial configurations for these runs, taken from the 298 K control simulations, were thermalized at 498 K by rescaling atomic velocities every 0.1 ps with a Berendsen thermostat during 500 ps before starting production runs. From the simulations at these thermodynamic conditions, we were able to investigate the early stages of the LBD denaturation, but not the complete unfolding and expansion of the protein hydrophobic core.

An additional set of simulations, reaching higher temperatures, has been performed in order to observe the complete denaturation of the LBDs accompanied by the actual expansion of the hydrophobic core. For that, temperatures around and above 650 K were necessary in order to promote full unfolding during the typical length of our simulations. For these auxiliary runs, we have chosen to computationally promote full denaturation by progressively heating the system. This approach differs from conventional, fixed temperature, protein denaturation simulations since kinetic and thermodynamic aspects are convoluted. The heating was such that the temperatures around which denaturation is observed were rapidly reached, but subsequently varied less steeply. In this way, we were able to promote a broader sampling of the conformational space as the mobility of the protein increases. Therefore, starting from 298 K the temperature was scaled at each 1.5 ps according to the equation: $T = 298 + 5(t/1.5\text{ps})^{1/2}$ where T is the temperature in Kelvin and t is the simulation time in ps. Four independent auxiliary simulations were performed for different systems, namely: Triac-TRα and Triac-TRβ complexes and TRα and TRβ without Triac. For simulations of apo-structures, the models were equilibrated at 298 K for 2 ns before heating because the protein structural

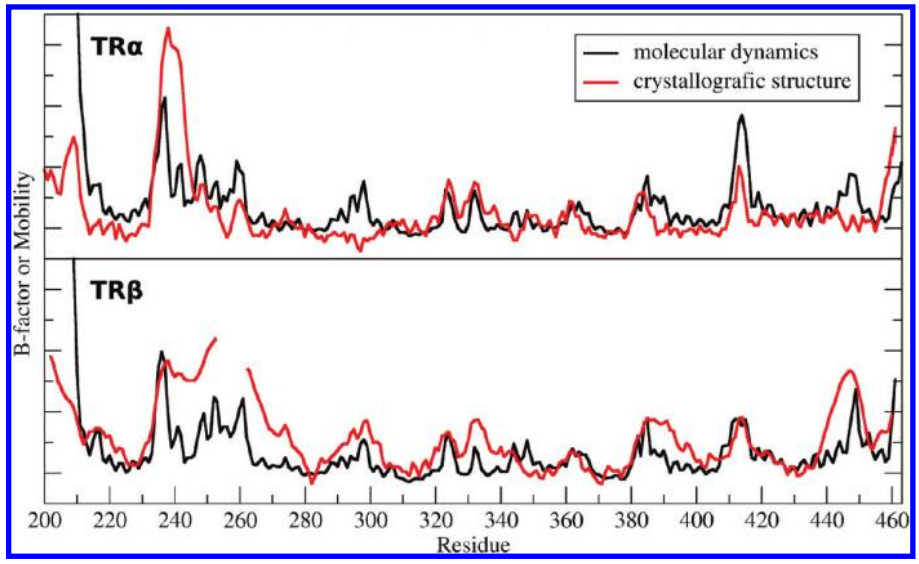

Figure 2. Temperature B-factors obtained from the TRα and TRβ crystal structures and computed values relative to the averaged structures obtained from the 20 ns control simulations, in arbitrary units. The incomplete region of the red line corresponds to the Ω-loop, absent in the crystal structures.

models have been obtained from the ligand-bound structures (no structural models for the apo-forms of the TR LBDs are available to date). These simulations were performed with constant volume at a density equals to that of liquid water at 298 K.

The protein structure and dynamics were characterized by the following order parameters: (1) the secondary structure, which was computed using STRIDE[46] for each frame; (2) the radius of gyration (R_g); (3) the root-mean-square deviations (rmsd's) for Cα atoms, computed by aligning each frame to the initial structure with the algorithm described by Kearsley;[47] (4) the native contacts, which were defined between two residues if, in the native structure, their Cα atoms were less than 7 Å apart. For this calculation, a list of contacts was obtained for each residue during the course of the simulation starting from the first frame, thus generating a time-history for the number of native contacts; (5) the protein solvation level, computed by counting the number of water molecules in the first solvation shell around the protein. A water molecule was considered in the first solvation shell if any of its atoms were less than 4 Å apart from any atom of the protein.

3. Results and Discussion

A. Experimental Measurements of the Effect of Ligand Binding on Protein Thermal Stability. The CD spectra of purified TRα and TRβ LBDs are typical of proteins containing elements of α-helical secondary structure, characterized by two negative bands at 208 and 222 nm. The thermal stabilities of the TRα-Triac and TRβ-Triac complexes, and of the apo-LBDs were experimentally investigated by far-UV CD spectroscopy as a function of the temperature (see Material and Methods). This can be readily followed by accompanying the ellipticity at 222 nm, which is the dominant peak characteristic of α-helical structure and falls within a region of the spectrum where the signal-to-noise ratio is high. The analyses were performed by fitting the data to a two-state transition. The best fitting parameters T_m and apparent enthalpies of the unfolding transition are presented in Table 1. Triac was chosen because it is the ligand that promotes the greatest stabilization among several TR ligands in preliminary denaturation experiments.[26] Figure 3 panels a and b show the thermal unfolding transitions for TRα and TRβ LBDs in the absence (apo) and presence (holo) of Triac. In the absence of Triac, the spectral profiles of the recombinant TRα and TRβ LBDs remain relatively constant below 310 K and are progressively altered as the temperature increases above 310 K, with a loss of definition of the α-helix characteristic minima at 222 nm. Triac binding stabilizes the TRα LBD, increasing the melting temperature (T_m) in approximately 9 deg (from 317 to about 327 K, see Table 1). The stabilizing effect of Triac on TRβ is more prominent, as shown in Figure 3b. Triac induces a higher increase in the protein thermal stability, and the values determined for the melting temperature are $T_m = 330$ K for TRβ-Triac complex and $T_m = 315$ K for apo-TRβ. The larger stabilization effect promoted by Triac on the β subtype is correlated with the β-selectivity of Triac.[26] No unfolding intermediates are distinguishable from the CD signal for TRα or TRβ, with or without ligand. This suggests that the LBD unfolding is highly cooperative. The denaturation profiles of the apo- and holo-TRβ LBD exhibit steeper slopes than the TRα counterparts, indicating that the TRβ LBD is more cooperative than the TRα LBD, as monitored by the increase in the apparent enthalpy of unfolding (Table 1), both with and without ligand (a vertical slope indicates a fully cooperative two-state transition). Similar profiles showing cooperative unfolding were obtained for the estrogen receptor-α LBD.[39] Different experimental techniques also indicate that the peroxisome proliferator-activated (PPAR) LBD structure is also highly cooperative.[48]

TABLE 1: Effect of Triac on the Thermal Unfolding of TRα and TRβ LBDs. Data Were Fit as Described in the Materials and Methods

	apo		holo	
	T_m (K)	ΔH (kcal/mol)	T_m (K)	ΔH (kcal/mol)
TRα LBD	317.5 ± 0.5	37 ± 3	326.9 ± 0.3	66 ± 6
TRβ LBD	315.5 ± 0.3	55 ± 4	330.2 ± 0.3	96 ± 10

From these experiments alone one cannot obtain molecular level information about how Triac stabilizes the LBD. One may hypothesize, for instance, that the ligand stabilizes solely the folded state and that denaturation would proceed from the apo-LBD, after the ligand has dissociated from the protein core (say, promoted by the initial temperature rise). Alternatively, one could

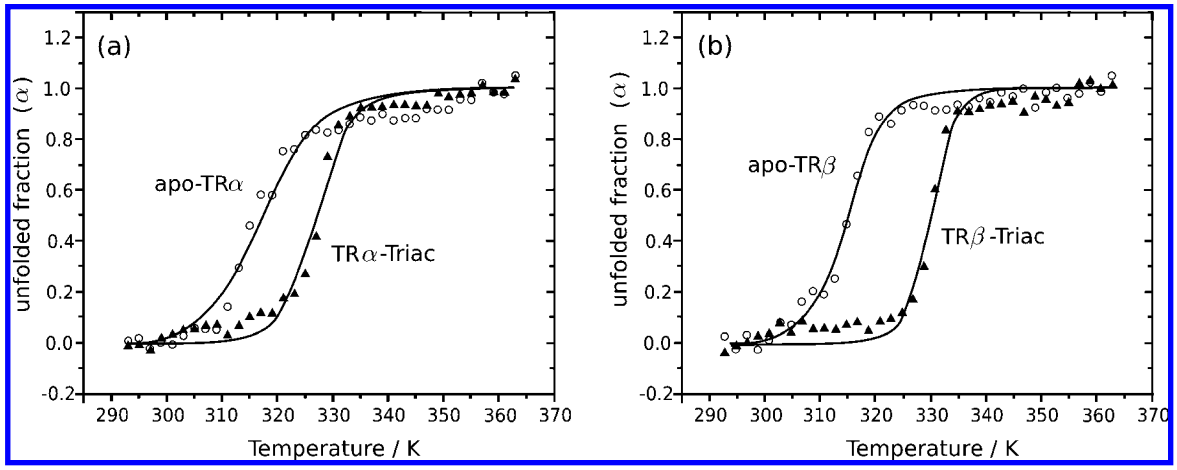

Figure 3. Temperature induced denaturation experiments of the LBDs of TRs as measured by circular dichroism at 222 nm: (a) apo- and Triac-bound TRα LBD; (b) apo- and Triac-bound TRβ LBD. Protection of the LBD from denaturation by Triac is subtype specific.

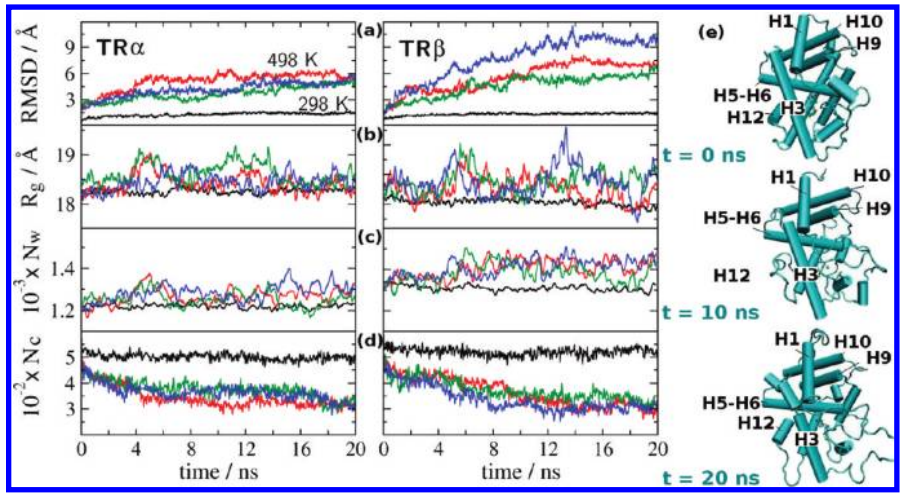

Figure 4. Structural parameters of the TRα (left panels) and TRβ (right panels) LBDs bound to Triac in control and high-temperature simulations. Computed quantities are (a) the root-mean-square deviations (rmsd) of Cα atoms, (b) the radii of gyration (R_g), (c) number of water molecules in the first solvation shell around the protein (N_W), and (d) number of native contacts (N_C). (e) Also shown are representative snapshots of a 498 K TRβ run illustrating structural unfolding within a compact LBD.

argue that the ligand may remain bound to a partially unfolded structure, thus stabilizing the intermediates of the denaturation processes. These are two very distinct hypothetical unfolding scenarios which cannot be discerned from the present experiments. As we shall see, the simulations presented here support the view that denaturation proceeds through the formation of a molten globule state which preserves a hydrophobic core and, therefore, is still able to interact effectively with the ligand.

B. Denaturation Events at 498 K. Nine independent 20 ns simulations of the denaturation of TRα and TRβ at 498 K were performed. The structural characteristics of the LBDs during these simulations are compared with control simulations performed at 298 K. Figure 4 shows the rmsd of Cα carbon atoms of the TRα-Triac (left panels) and TRβ-Triac (right panels) LBD complexes at the two temperatures. At 298 K the rmsd's relative to the initial structures oscillate only slightly around an average value of 1.4 Å, indicating that the LBD structures are stable at this temperature and display only local fluctuations. In contrast, the rmsd's of the Cα atoms during the simulations at 498 K increase systematically to more than 6 Å in all independent runs. The increase in the rmsd at 498 K indicates that important conformational drifts relative to the initial structures took place. Furthermore, the rmsd's increase steadily in all runs (more sharply up to ~13 ns and leveling off at longer times), therefore indicating that the structures continue to deviate from the native state. The rmsd of the β isoform at 498 K increases slightly above that of TRα due to the motions of the β-sheets, which are more prominent in the former.

At the same time, the variation of the radius of gyration (R_g) reveals only a modest expansion of the LBDs during the 498 K simulations. At 298 K the radius of gyration oscillates mildly around an average value of 18 Å. During the course of the 498 K simulations the maximum value of R_g observed was 19.6 Å (8% greater than at 298 K), but it oscillates around 18.6 Å most of the time, representing only some 3% increase relative to the average R_g of the control run. Most notable, however, is the fact that the radii of gyration do not increase systematically during the high-temperature simulations in either LBD subtypes. The relatively modest expansion of the structure had occurred essentially during the initial thermalization stage at the beginning of each run and remains oscillating around a constant value thereafter. For example, the maximum value of R_g is obtained for one of the TRβ runs at 498 K (Figure 4, right, blue curve) at 12.7 ns of simulation. For the same run, R_g also attains the smallest value of all simulated systems at a later time (~18 ns of simulation). These results show that the expansion of the structures as indicated by the radius of gyration is not correlated with the increase of the rmsd. Therefore, the simulations suggest that unfolding must be a consequence of internal rearrangements of the structure, yet preserving the LBD fold density.

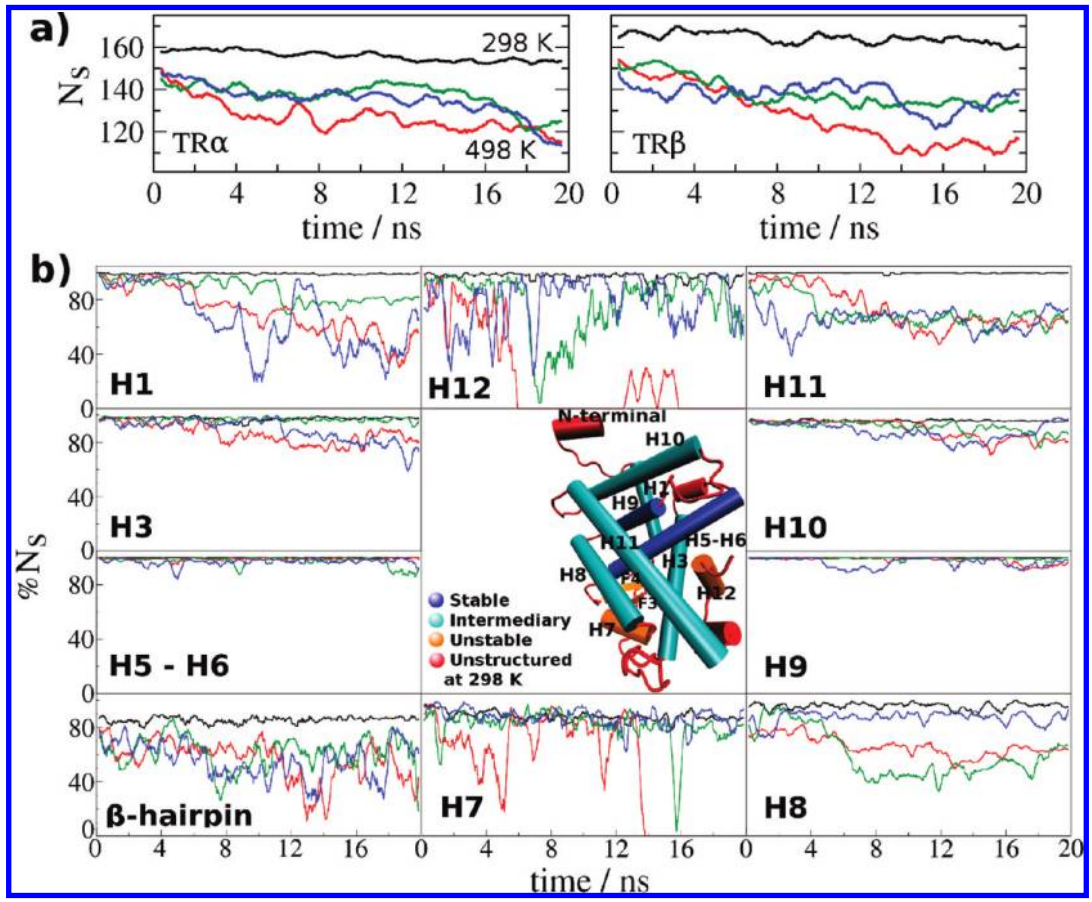

Figure 5. Content of secondary structure of the liganded TR LBDs: Global α-helical content of TRα (a) and TRβ (b) at 298 and 498 K. (c) Percentage of preserved secondary structure in each structural element of the LBD (black lines, 298 K; color lines, 498 K). The center panel shows the TRβ structure and summarizes the results of this figure. The most stable secondary structure elements are H5, H6, and H9 (blue), followed by H1, H3, H8, H10, and H11 (cyan), which show partial loss of helical structure at 498 K runs.

Other structural parameters are consistent with the above interpretation. The solvation of the LBD, as measured by the number of water molecules within 4 Å shells around protein residues, increases about 10% within first 5 ns of simulation, and then remains, on average, constant (Figure 4c). Here again one sees that the level of residue hydration is somewhat higher for TRβ, which is in part responsible for the β selectivity of Triac.[26] The solvent accessibility of the LBD resembles the expansion of the structures as given by the time evolution of the radii of gyration, but not the increase observed in the rmsd. In contrast, the number of native contacts decreases steadily for all runs at 498 K (Figure 4d), indicating internal rearrangements of the structure. Three representative snapshots were extracted from a 498 K run of the TRβ-Triac complex and are displayed in Figure 4e. Consistently with the structural order parameters, the snapshots suggest that the structure is unfolding without losing its globular character. The formation of a molten-globule state is thus characterized. Although we cannot rule out putative pressure effects in the maintenance of the globular shape in these simulations, it is worth pointing out that simulations of staphylococcal nuclease conducted at 8 kbar and 298 K have shown that high pressure did not prevent expansion of the protein structure, which was characterized as an early stage of the denaturation process.[36]

Figure 5a shows the secondary structure of the protein as function of time during the 20 ns runs at 498 K. For comparison, results from the control simulations at 298 K are also shown. The native structure is formed mostly by α-helices, and contains only four small β-sheets (Figure 1). Therefore, we monitor the secondary structure by the α-helical content. At 298 K, α-helices comprise about 160 residues in the native fold. Roughly 5% of the secondary structure is very unstable at 498 K, being lost during the 500 ps thermalization runs for both isoforms. Further secondary structure is lost during the high-temperature simulations, but at least 100 residues preserve their α-helical conformation during the entire course of the simulations in all cases. Both LBD subtypes lose secondary structure with similar rates. There are greater variations in the behavior of N_S for different simulations of the same subtype than between distinct isoforms. The same applies to the results shown in Figure 4, discussed above, indicating that the subtype specific unfolding observed experimentally could not be resolved by the present simulations.

The time-history of distinct secondary structure elements of the LBD were monitored independently. Results are shown for TRβ in Figure 5b. At 298 K, only small potions of F1, H2, H4, and the N-terminal domain lack secondary structure (not shown). At 498K runs, these parts of the molecule were almost totally unstructured. Significant losses of secondary structure are also observed in almost all other helices, particularly H1, H8, H11, and H12, followed by helices H3 and H7. H1 loses 40% of its native secondary structure content, H11 loses about 35%, and H12 loses more than 35%. In one of the simulations, the secondary structure of H12 has been completely lost. H3 loses about 25% of its helical arrangement, H7 around 20% (fully unwinding in one of the runs), and H8 loses up to 40% of its helical content. Not surprisingly, the β-hairpin also loses secondary structure in all cases.

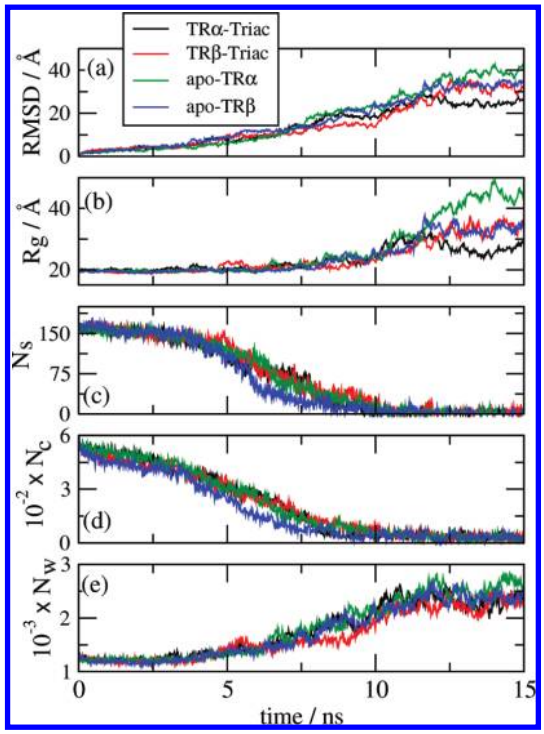

Figure 6. Structural parameters as a function of time for the continuous heating runs: (a) rmsd, (b) radius of gyration, (c) α-helical content, (d) fraction of native contacts, (e) hydration number.

The most resilient helices are H5, H6, H9, and H10. H10 loses at most 20% of its native helical structure, H9 remains more than 95% preserved, and almost no denaturation is observed in helices 5 and 6 (which behave as a single helix in control and denaturation simulations). H5, H6, and H9 are, therefore, the most stable secondary structure elements and, not surprisingly, form the inner core of the LBD. The center panel in Figure 5b provides an overall view of these results by color-coding the LBD according to the relative resilience to thermal denaturation of its different structural elements.

C. Full Denaturation Runs. To observe complete denaturation events and to verify some of the main conclusions drawn from the 498 K simulations using a different simulation protocol, we have performed auxiliary simulations of the TR LBDs by gradually increasing the temperature from 298 to 800 K, as described in Materials and Methods. At 800 K, the LBD was completely unstable during short trial simulations.

Full denaturation of the LBDs was reached during these simulations, as evidenced by the structural indicators depicted in Figure 6. The fraction of native contacts approaches zero, the rmsd of all structures becomes greater than 25 Å, all secondary structure elements are lost, and the residues are completely hydrated. The radii of gyration increase to more than 25 Å in all structures, reaching a maximum of 50 Å for the apo-TRα simulation. This suggests that the proteins have reached a random-coil state during these simulations. The profiles of these structural indicators as functions of simulation time support the view of the initial denaturation stages provided by the 498 K simulations. Namely, at 6 ns of simulation (when the temperature reaches ~685 K), about 30% of the α-helical content is lost for all structures, the rmsd's approach 10 Å, and only 40% of the native contacts persist. Yet, only small increases in the radius of gyration are observed (at 6 ns, the R_g values are only slightly greater than the initial value of 20 Å). The radius of gyration undergoes a sharp increase only after approximately 9 ns (~772 K) of simulation, when there is almost no residual native fold, as inferred from the fraction of native contacts, N_C, (Figure 6d) and the α-helical content, N_S, (Figure 6c). At this temperature, the rmsd's of all structures are still below 25 Å. The extent of residue hydration is also well correlated with the expansion of the structure, since significant increase in the hydration level of the residues appears only as the protein expands.

Therefore, these simulations indicate, like the constant temperature runs at 498 K, that the molten-globule state of the LBD is preserved while the secondary structural elements denature by internal rearrangements. Part of the secondary structure of the LBD is lost before the expansion of the hydrophobic core. This expansion is then accompanied by the loss of more stable secondary structure elements leading to the final stages of the denaturation. The denatured state is composed of small elements of secondary structure contained in a mostly globular arrangement of random coils. This model is different from the unfolding mechanisms described for most other proteins for which molecular dynamics simulations have been performed. These differences are due to the size of the proteins and the hydrophobicity of the protein core. The loss of native tertiary contacts and the denaturation of secondary structure elements that are totally buried within the protein occur simultaneously, while the expansion of the structure occurs afterward. This behavior is similar to that experimentally observed for the Barstar protein[32] and contrasts the case of smaller proteins, particularly small α-helical proteins,[30,36] with small hydrophobic cores, which tend to lose compactness before most secondary structure denatures.

To provide further view into the molecular events culminating with the complete denaturation of the LBD, we have depicted in Figure 7 a few trajectory snapshots of the TRβ-Triac structures taken at different stages of the full denaturation runs. The movement of the Ω-loop is the first notable step of denaturation, clearly observed when the temperature increases from 572 to 581 K. This displacement is readily accompanied by the denaturation of the β-hairpin. At 590 K there is a significant loss of secondary structure in H1 and that H8, H11, and H12 have been affected. H8 and H11 were displaced from each other, and the denaturation of the C-terminal end of H11 becomes evident. When the temperature reaches 606 K, H3 becomes significantly unwound. The bottom of the protein, including H12, is almost totally unstructured. The ligand has not left the structure, and while its native contacts are greatly affected, its orientation in the structure is still somewhat preserved. From 622 to 658 K there is a progressive unwinding of other secondary structure elements. At 622 K important secondary structure elements, particularly H6 and H9, still remain. H11 is also mostly preserved, but H10 seems to be lost. At 644 K, H11 is lost, whereas the presence of residual secondary structure from the inner helices, such as H6 and H9, is apparent. The ligand is displaced from its original position and leaves the receptor at 658 K. From then on, the top part of the receptor continues to exhibit some secondary structure, which becomes only residual at 695 K. The overall structure is a molten globule which is not expanded until higher temperatures are reached.

These results can be put into a more quantitative basis by comparing the compactness and secondary structure content for different regions of the LBD. The compactness factor, $C_{C\alpha}$, around an individual residue is computed for each Cα atom according to the expression $C_{C\alpha} = \sum_{C\alpha'}(1 + d_{\alpha\alpha'}{}^2)^{-1}$, where the sum extends to all other Cα′ atoms of the protein, except the ones closer than four residues from the reference Cα along

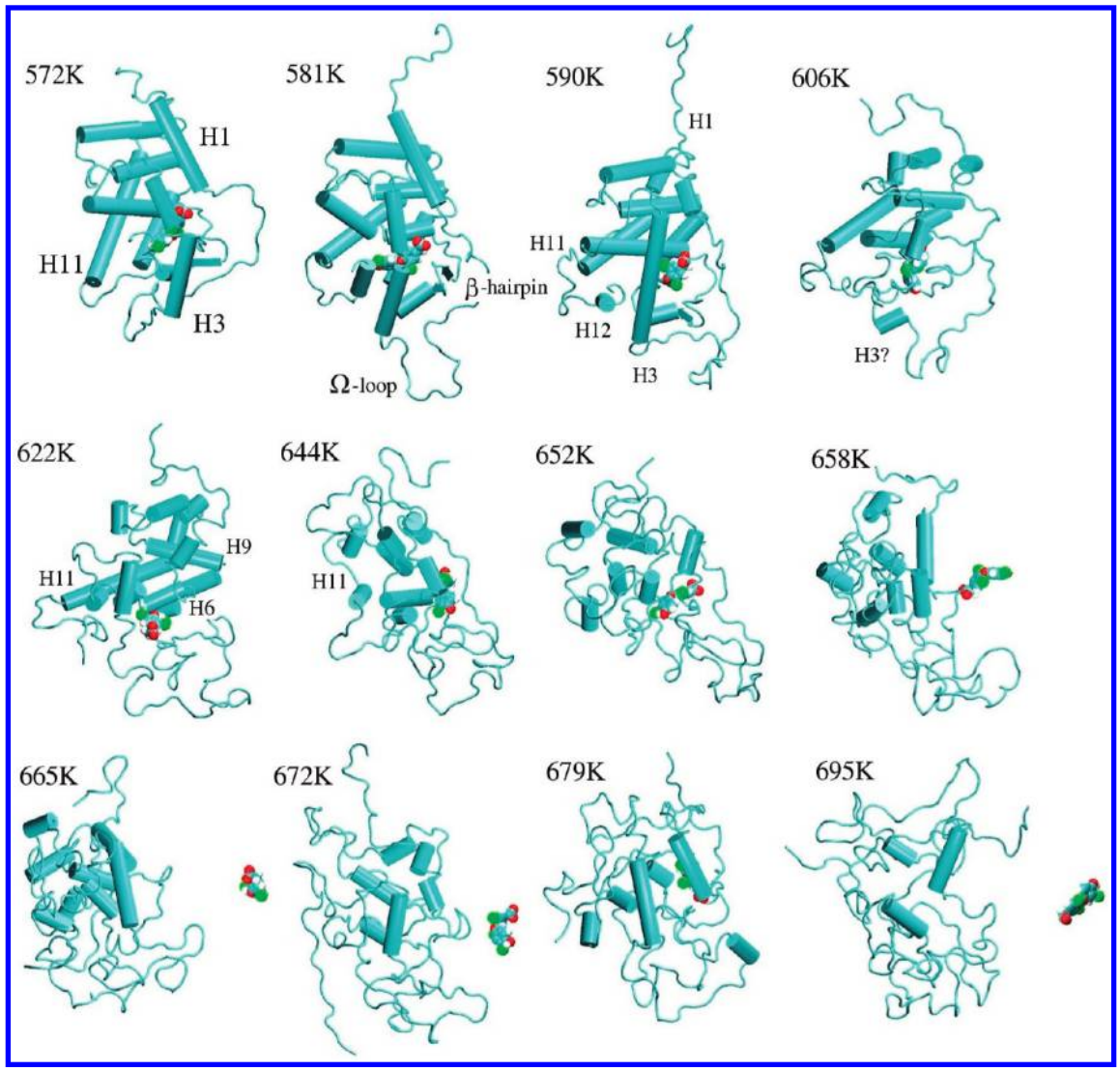

Figure 7. Snapshots of the denaturation of TRβ bound to Triac during continuous heating runs.

the protein sequence, and $d_{\alpha\alpha'}$ is the distance between a pair of Cα atoms. This parameter is large for a given Cα if there are several other Cα atoms spatially close to it, indicating a compact tertiary structure. As the protein unfolds, $C_{C\alpha}$ must decrease, since the tertiary structure is lost and the protein becomes less compact. Figure 8 shows the compactness factor and the level of secondary structure for the Triac-TRβ complex. Similar results are obtained for the other three systems (apo-TRβ, apo-TRα, and holo-TRα) and are presented as Figures S1, S2, and S3 in the Supporting Information. From the evolution of the compactness factor we see that two regions are affected very early in the simulation: The hinge before H1 and the coil between H2 and H3, which includes the Ω-loop. The regions that remain compact for most of the time are H1, the end of H3, H6, H9, and to some extent the region comprising H11. The secondary structure is more stable for H1, the end of H3, H6, and H9.

For TRβ in the absence of ligand, most elements of the secondary structure denature faster, but particularly H1 which is lost before the first 6 ns of simulation. H9 and the N-terminal region of H11 emerge as the most stable secondary structures. For TRα, on the other hand, ligand binding appears to strongly stabilize H6, but the stabilization effect on H1 is not observed and H6 appears to be more stable than H9 (see Figure S3). H9 seems to be destabilized by the presence of the ligand in TRα in contrast to a greater relative stabilization of H6.

The elements that are first exposed (as measured by the compactness factor) are the hinge before H1 and the region between H1 and H3, particularly the regions comprising the Ω-loop and the β-hairpin. Secondary structure is rapidly lost for H4, H7, and H12, followed by the N-terminal region of H3, H5, H8, and some regions of H10. In TRα, H8 is as stable as H9, contrary to apo- and holo-TRβ structures, for which H9 is more stable. A more comprehensive analysis of the ligand effect upon protein folding could be obtained if crystallographic structures of the LBD without the ligand were available. Although we have equilibrated the apo structures for 2 ns before simulating their thermal denaturation, some of the events observed here may occur in physiological conditions not only during denaturation, but as a rearrangement of the structure in response to ligand dissociation.

Therefore, the most stable elements concerning all simulations are parts of H3, H6, H9, and the N-terminal region of H11. As we shall see in more detail below, ligand binding promotes stabilization particularly of H1 and H9 in TRβ and of H6 in TRα. The recurrent appearance of H6 and H9 as the most stable elements of the structure comes from the fact that the compact structure protects inner helices from denaturation to a higher

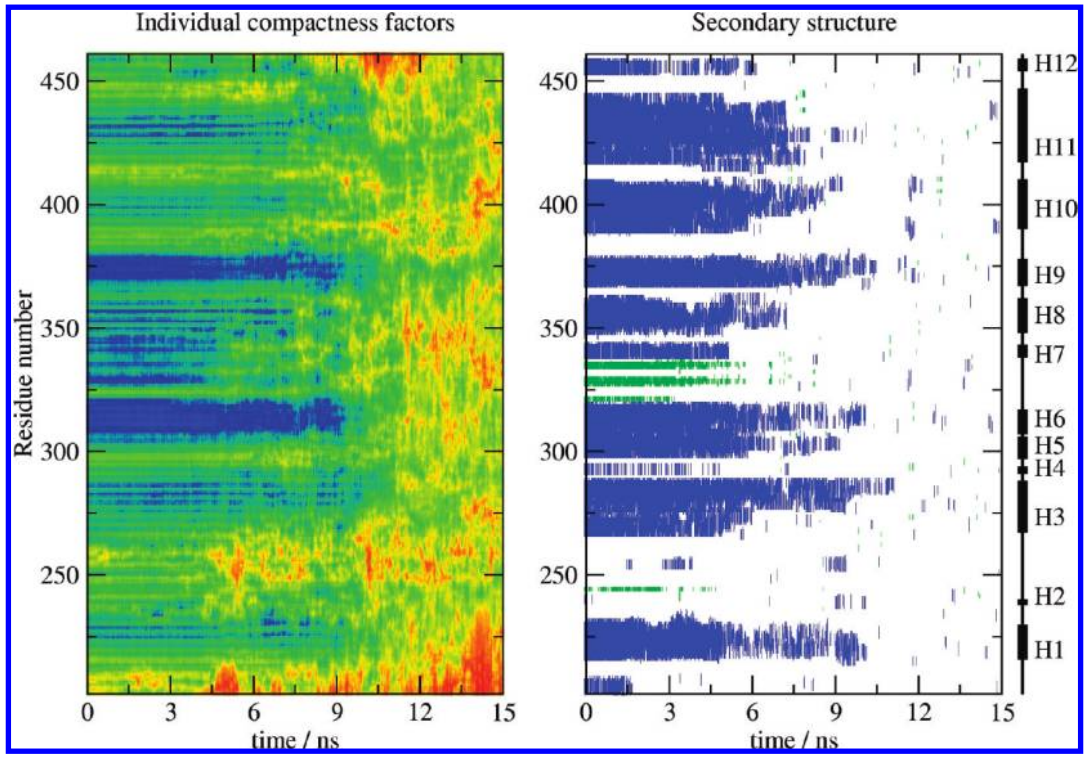

Figure 8. Denaturation maps for TRβ bound to Triac. The individual residue compactness factor, $C_{C\alpha}$, decreases from blue to red (left). The α-helical residues are blue and β-sheets are green in the secondary structure map (right).

extent. This has implications to the putative folding mechanisms, as discussed later.

D. The Role of Ligands. Experiments demonstrate that Triac has an important role in stabilizing the LBD toward denaturation. This has been previously observed for ER and PPAR LBDs, in addition to other experimental evidence that ligand binding leads to an overall more compact LBD.[49−51] For ER, in particular, it was experimentally demonstrated that the LBD can acquire a partially unfolded structure, which may bind and release ligands rapidly.[52] In the context of the present simulations, one can suggest that this partially unfolded state can be a molten-globule, with structured inner-core secondary structural elements. These elements, particularly H6 in the case of TRs, form native contacts with the ligand. Evidently not all native ligand-protein contacts are preserved during the 498 K simulations. In fact, in one of the 498 K runs performed in the presence of Triac, the ligand appears to be driven out of its native binding mode toward the exterior of the LBD through the region comprising the β-sheets and helice 3 (not shown). In this partially unfolded Triac/TRβ structure, the ligand's carboxylate group makes hydrophilic contacts with surrounding water molecules, resembling one of the ligand dissociation pathways encountered by previous MD simulations.[20−22]

The major unfolding events in the increasing-temperature simulations occur between 500 and 650 K (i.e., ~3 to 9 ns). Therefore, we analyzed the rmsd per residue in this section of the trajectories in order to obtain insights into the most important steps of denaturation and the role played by the ligand in the protein stabilization. Figure 9 depicts the rmsd per atom at four different temperatures in the range from 500 to 650 K, corresponding to simulation times of 3, 6, 7.5, and 9 ns.

For TRβ bound to Triac (Figure 9a) one can observe that at 521 K (3 ns), most of the structure has a rmsd lower than 10 Å; the structure is still similar to the native state. However, denaturation proceeds fast and at 572 K (6 ns) the residues from the N-terminal end, near H1, are significantly displaced from

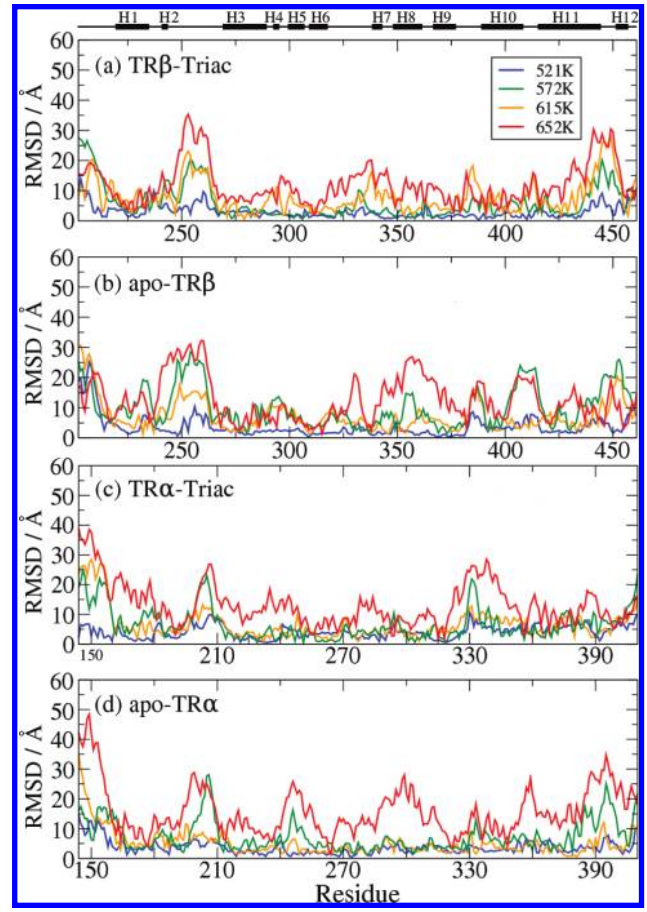

Figure 9. Root mean square deviation at selected temperatures of the LBD Cα atoms for (a) TRβ bound to Triac, (b) TRβ without ligand, (c) TRα bound to Triac, and (d) TRα without ligand.

their original position, as well as the loop between H2 and H3 (the Ω-loop), some regions before H7, and portions within H10

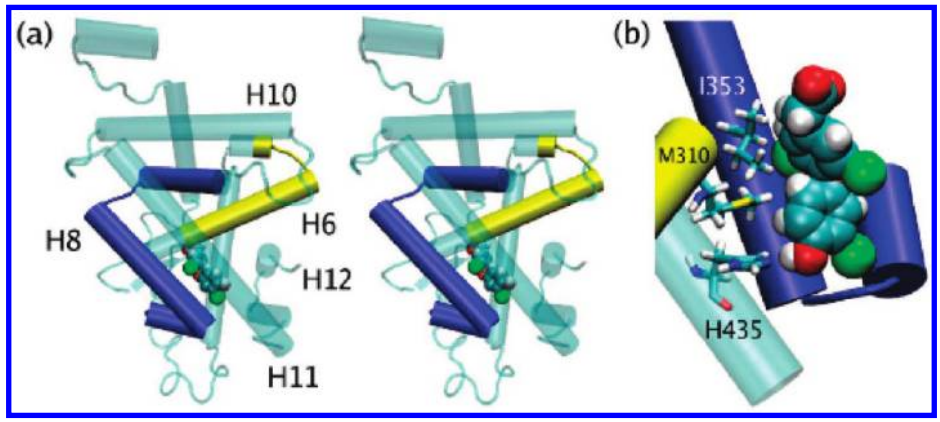

Figure 10. (a) Stereo view of the LBD structure with the regions for which the ligand appears to stabilize denaturation in blue for both α and β isoforms (helices H7−H9 and start of H10) and in yellow for TRα only (helices H5 and H6). (b) Details of the contacts that the ligand forms with H6 (yellow), H8 (blue), and H11 (cyan), that may explain why the ligand stabilizes the LBD toward denaturation.

and H11. A large deviation is also observed for the C-terminal portion of the protein, particularly the end of H11 and H12. Once the temperature reaches 615 K (7.5 ns) some of these structural deviations become more important, particularly in H4 and H5. The displacement of H7 becomes more apparent and the loops between H9 and H10, and the loop between H11 and H12 are distorted. At 652 K (9 ns) the Ω-loop (between H2 and H3) is highly mobile, the region concerning the loop between H6 and H7 is affected, and the mobility of the C-terminal portion of H11 becomes more important.

Figure 9b shows similar data for the denaturation of TRβ without ligand. The most important differences relative to the denaturation in the presence of ligand are that the loop between H6 and H7 does not appear to be as affected as in the holo-LBD simulation, except for a peak between residues Glu325 and Ala335. However, large rmsd's are observed in the region comprising H7, H8, and H9, which are much more affected by denaturation in the apo form of the LBD than in the Triac bound receptor. The loop between H10 and H11 seems to be destabilized in the absence of the ligand, and the loop between H11 and H12, on the contrary, has a smaller rmsd in the absence of ligand.

The denaturation of both holo and apo structures of TRα LBD shares many features with the denaturation of the TRβ structures. Large rmsd deviations are observed in the N-terminal region and for the Ω-loop between H2 and H3 (Figure 9c,d). Like in the β subtype, the region between H7 and H9 of TRα has become structurally more perturbed in the absence of the ligand in the later stages of this time window. The loop between H9 and H10 and most of H10 in the Triac bound TRα structure, however, exhibit higher values of rmsd in comparison to the other simulated systems.

Figure 10 highlights the substructures of the Triac bound TR LBD which are most affected during denaturation by the ligand binding. The region comprising H7−H9, stabilized by ligand binding in both isoforms, is shown in navy blue. H8, particularly, plays an important role in promoting the gain in stability of both isoforms upon ligand binding. A key step toward unfolding is the opening of the H8−H11 interface and the exposure of the ligand's hydrophobic pocket. The ligand interacts simultaneously with both H8 (with Ile353 in TRβ) and H11 (an important hydrophilic interaction with His435), as shown in Figure 10b, thus stabilizing the relative orientation of the two helices. In the absence of the ligand, H8 becomes more mobile and, along with it, so does H7 and H9.

The region that appears to be ligand-stabilized only in the TRα subtype is depicted in yellow (H5 and H6). Helix 6 appears to be one of the most stable secondary structure elements of all systems considered, but the displacement of H5 resulted in a higher mobility of H6 in the apo-TRα structure. In this region of the protein, the ligand forms a hydrophobic contact with Met310 (TRβ numbering), and the loss of this interaction results in greater mobility of the apo-structure. However, this effect was not observed for TRβ.

The reasons why the ligand promotes greater stabilization of TRβ relative to TRα remain elusive. From the experimental data, we first noticed that TRα, in the absence of ligand, appears to be slightly more stable than TRβ. However, upon ligand binding, the melting temperature of TRβ becomes as much as 15 degrees higher than the melting temperature of TRα. Some regions of TRβ, particularly the region between H1 and H3 (containing the β-hairpin), and the Ω-loop, have greater mobilities relative to TRα, as indicated by temperature factors in crystallographic models.[9,14] Mobile regions have already been shown to drive the first stages of denaturation in other proteins,[29,30] and this may explain why the onset of TRβ denaturation occurs at a slightly smaller temperature than TRα in the absence of ligand. One hypothesis as to why the stabilization effect of the ligand may be greater on TRβ relative to TRα is related to the mobility of Ω-loop and its role in the stabilization of the H8−H11 interface. In contrast with the TRβ isoform, the Ω-loop in the TRα model appears to be compactly folded over the structure of the LBD, forming interactions with both the N-terminal end of H8 and the C-terminal region of H11. Therefore, in TRα there is already a stabilizing factor for the Ω-loop which is absent in TRβ because of the high mobility of the Ω-loop in this isoform. Thus, if the ligand represents an important factor in the stabilization of this interface, the relative importance of the effect should be greater for TRβ. Nevertheless, if this were the only factor, the absolute stability of TRα should still be greater for the liganded structures.

The aperture of the H8−H11 interface and the high mobility of H12 provide further insight into the mechanism of ligand-induced stabilization. As shown in Figure 11, the ligand protects H6 from the solvent in both structures, particularly in TRα. The ligand prevents water from solvating H6 by blocking water from entering the apertures formed by the displacement of H8, H11, and H12. The solvation of H6 is very likely a key step toward denaturation since H6 is an inner, hydrophobic helix. The protection of the inner core of the protein from hydration may provide stabilization for both isoforms in a similar fashion.

The second region of high mobility, as judged by temperature factors in crystallographic models, comprises the area between H1 and H3. This region is more likely affected by differences

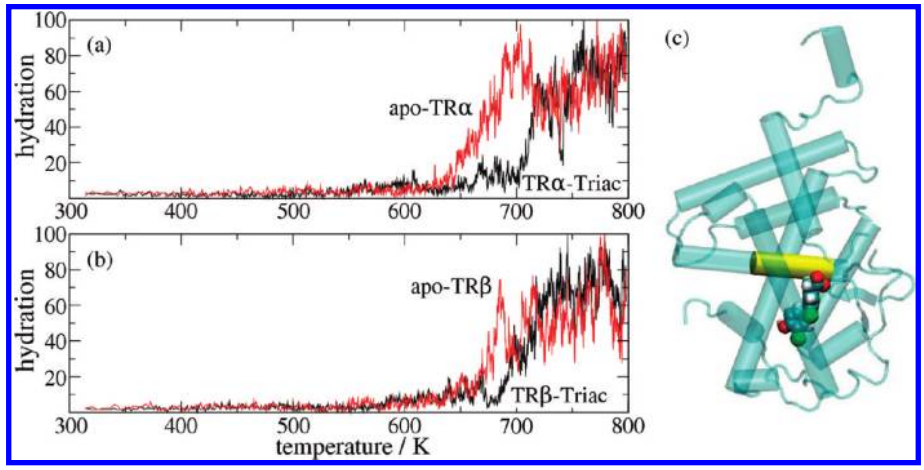

Figure 11. The ligand provides shielding to helix H6 hydration during unfolding in (a) TRα and (b) TRβ. This can explain part of the stabilizing effect of the ligand on both structures. In panel c, the residues of H6 considered here are highlighted in yellow.

in ligand binding affinity, which were generally observed to be related to the Asn277Ser active-site mutation. This mutation was shown to play a key role in the ligand binding affinity by promoting the formation of a local network of hydrogen bonds and affecting ligand mobility.[9,25,26] In both cases, it seems that ligands with greater affinity toward TRβ promote the stabilization of the loop between H1 and H2 and the β-hairpin. Indeed, for all simulated structures the detachment of H1 from the core of the LBD is seen as an important step toward unfolding. Thus, according to this view, the stabilization of the loop between H1 and H2 through selective ligand binding may provide the greatest overall contribution to the stability of the liganded TRβ structure.

Curiously, a study on PPARγ have shown that H1 and its interactions to H8 (correspondent to H9 in TRs) are critical for the receptor's stability.[48] The reported experiments corroborate with the notion of a highly cooperative structure, in which regions far from the ligand are required for and affected by ligand binding. It is interesting that one of these regions (H8 in PPARγ, H9 in TRs) was observed to have different dynamics in the presence and absence of ligand in our simulations. Furthermore, although no clear differences were observed for the dynamics of H1 resulting from ligand binding, part of H1 is one of the most mobile regions in all simulations performed here, supporting the above-mentioned view regarding the effect of ligand on the stability of the LBD. A complete elucidation of the structural reasons behind the differential stability of each TR isoform bound to Triac will require, however, additional experimental or theoretical studies.

E. Insights into LBD Folding Mechanism. It is usually assumed that the mechanisms of protein denaturation may provide insights into the mechanisms of protein folding due to the principle of microscopic reversibility.[28,53,54] Folding to the native structure probably occurs stepwise, by the initial arrangement of substructures. These reorganize into the complete folded protein, avoiding a random search in phase space.[53,54] The secondary structure elements are clearly the most plausible candidates for being the first emerging structural motifs, particularly for α-helical proteins.[30]

The LBDs of TRs are relatively large and contain several entire secondary structure elements protected from solvent, which may not be stable when fully exposed to water. With this in mind, our simulations suggest that the folding of the LBD would occur first by the collapse of the hydrophobic residues forming an unstructured hydrophobic core (this resembles the folding mechanisms observed in the microsecond time-scale for the significantly smaller protein, villin headpice subdomain[55]). The hydrophobic collapse would provide the required environment for the inner core secondary structure elements to be formed (H5, H6, and H9, the most resistant to denaturation). By taking the inner helices as templates, it is plausible that the secondary structure elements of the protein surface are formed in positions resembling their relative orientation to the native LBD.

4. Concluding Remarks

The LBDs of NRs are fundamental for ligand binding, dimerization, and cofactor recognition.[6] There is a growing body of evidence revealing the fundamentals of the folding and stability of NR LBDs, but there are only a few studies reported on the nature of their folding pathways.[39,48,50−52] There is evidence that the structure and dynamics of the PPARγ and ER LBDs are highly cooperative in the sense that each structural motif is required for the stability of the other elements of the structure.[39,48] For ER, furthermore, it was recognized that partially unfolded states facilitate binding without the exposure of the protein core to solvent.[51] In the context of the present work we could interpret these partially unfolded states as globular arrangement of unwound secondary structure elements with native overall topologies. For TRs, in particular, mutational studies provide information about which regions of the protein are required for protein activity or stability, but the actual functional roles of the mutated residues and their relationship with the dynamics of the receptor are still largely unknown.

In the present work we report circular dichroism spectroscopy data that corroborates the well-known stabilizing effect of Triac on the structure of the LBD of TRs. The experiments show that significant stabilization is promoted by ligand binding, and to different degrees in each TR subtype. We have also presented here the first molecular dynamics simulations of the denaturation mechanisms of the LBD of nuclear receptors. The simulations indicate that the unfolding mechanisms of the LBD occur by the denaturation of the secondary structure at the same time or prior to the expansion of the hydrophobic core. Furthermore, the ligand presumably does not fully dissociate from the protein until the LBD is conformationally distorted, which seems consistent with the ligand stabilizing effects in denaturation experiments. The inner α-helices, which are mostly hydrophobic, seem to be the most stable elements of the structures. The ligands affect denaturation by stabilizing the interface between H8 and H11, an effect that in principle should affect both TRα and TRβ, but the latter to a greater extent. The presence of the

ligand appears to protect inner helices, particularly H6, from exposure to solvent.

Although the simulations have been carried out at much higher temperatures than the experiments, which is a drawback for a detailed analysis of the processes, they provide the first molecular level description of the unfolding mechanisms of NRs in general. Our findings may have relevant implications for the interpretation of available experimental data, since the preservation of the compactness of the structure we encounter in our simulations can explain how ligands may bind to partially denatured states.[52] From the point of view of protein folding in general, this study provides a picture of the denaturation mechanisms and possible folding pathways of a compact α-helical protein, which is relatively large compared with other proteins currently studied by molecular dynamics simulations. The denaturation mechanisms observed are ligand-dependent and nontrivial in the context of available studies of protein denaturation. The folding of the LBD is proposed to occur initially by a hydrophobic collapse and the formation of the inner elements of secondary structure, which may provide templates for the formation of the external helices already in their native relative orientations.

Acknowledgment. We thank the Brazilian agencies CNPq and FAPESP (Grants 06/00182-8 to I.P and M.S., and 06/06831-8 to L.M.) for financial support.

Supporting Information Available: Further details on the time evolution of the denaturation maps for apo-TRβ, apo-TRα and Triac-TRα complex structures. This material is available free of charge via the Internet at http://pubs.acs.org.

References and Notes

(1) Evans, R. M. *Science* **1998**, *240*, 889.
(2) Bain, D. L.; Heneghan, A. F.; Connaghan-Jones, K. D.; Miura, M. T. *Annu. Rev. Physiol.* **2007**, *69*, 201.
(3) Tsai, M. J.; O'Malley, B. W. *Annu. Rev. Biochem.* **1994**, *63*, 451.
(4) Gronemeyer, H.; Gustafsson, J. A.; Laudet, V. *Nat. Rev. Drug Discovery* **2004**, *2*, 950.
(5) Webb, P. *Expert Opin. Investig. Drugs* **2005**, *13*, 489.
(6) Ribeiro, R. C. J.; Kushner, P. J.; Baxter, J. D. *Annu. Rev. Med.* **1995**, *46*, 443.
(7) Wagner, R. L.; Apriletti, J. W.; McGrath, M. E.; West, B. L.; Baxter, J. D.; Fletterick, R. J. *Nature* **1995**, *378*, 690.
(8) Yen, P. *Physiol. Rev.* **2001**, *81*, 1097.
(9) Wagner, R. L.; Huber, B. R.; Shiau, A. K.; Kelly, A.; Lima, S. T. C.; Scanlan, T. S.; Apriletti, J. W.; Baxter, J. D.; West, B. L.; Fletterick, R. *J. Mol. Endocrinol.* **2001**, *15*, 398.
(10) Ye, L.; Li, Y. L.; Mellstrom, K.; Mellin, C.; Bladh, L. G.; Koehler, K.; Garg, N.; Garcia Collazo, A. M.; Litten, C.; Husman, B.; Persson, K.; Ljunggren, J.; Grover, G.; Sleph, P. G.; George, R.; Malm, J. *J. Med. Chem.* **2003**, *46*, 1580.
(11) Dow, R. L.; Schnelier, S. R.; Paight, E. S.; Hank, R. F.; Chiang, P.; Cornelius, P.; Lee, E.; Newsome, W. P.; Swick, A. G.; Spitzer, J.; Hargrove, D. M.; Patterson, T. A.; Pandit, J.; Chrunyk, B. A.; LeMotte, P. K.; Danley, D. E.; Rosner, M. H.; Ammirati, M. J.; Simons, S. P.; Schulte, G. K.; Tate, B. F.; DaSilva-Jardine, P. *Bioorg. Med. Chem. Lett.* **2003**, *13*, 379.
(12) Borngraeber, S.; Budny, M.-J.; Chiellini, G.; Cunha-Lima, S. T.; Togashi, M.; Webb, P.; Baxter, J. D.; Scanlan, T. S.; Fletterick, R. J. *Proc. Natl. Acad. Sci. U.S.A.* **2003**, *100*, 15358.
(13) Sandler, B.; Webb, P.; Apriletti, J. W.; Huber, B. R.; Togashi, M.; Cunha-Lima, S. T.; Juric, S.; Nilsson, S.; Wagner, R. L.; Fletterick, R. J.; Baxter, J. D. *J. Biol. Chem.* **2004**, *279*, 55801.
(14) Nascimento, A. S.; Dias, S. M.; Nunes, F. M.; Ambrosio, A. L. B.; Aparicio, R.; Bleicher, L.; Figueira, A. C. M.; Neto, M. D.; Santos, M. A. M.; Fischer, H.; Togashi, M.; Craievich, A. F.; Garratt, R. C.; Baxter, J. D.; Webb, P.; Polikarpov, I. *J. Mol. Biol.* **2006**, *360*, 586.
(15) Renaud, J. P.; Rochel, N.; Ruff, M.; Vivat, V.; Chambon, P.; Gronemeyer, H.; Moras, D. *Nature* **1995**, *378*, 681.
(16) Nolte, R. T.; Wisely, G. B.; Westin, S.; Cobb, J. E.; Lambert, M. H.; Kurokawa, R.; Rosenfeld, M. G.; Wilson, T. M.; Glass, C. K.; Milburn, M. V. *Nature* **1998**, *395*, 137.
(17) Bledsoe, R. K.; Montana, V. G.; Stanley, T. B.; Delves, C. J.; Apolito, C. J.; McKee, D. D.; Consler, T. G.; Parks, D. J.; Stewart, E. L.; Wilson, T. M.; Lambert, M. H.; Moore, J. T.; Pearce, K. H.; Xu, H. E. *Cell* **2002**, *110*, 93.
(18) Blondel, A.; Renaud, J. P.; Fischer, S.; Moras, D.; Karplus, M. *J. Mol. Biol.* **1999**, *291*, 101.
(19) Kosztin, D.; Israilev, K. S.; Schulten, K. *Biophys. J.* **1999**, *76*, 188.
(20) Martínez, L.; Sonoda, M. T.; Webb, P.; Skaf, M. S.; Polikarpov, I. *Biophys. J.* **2005**, *89*, 2011.
(21) Martínez, L.; Webb, P.; Polikarpov, I.; Skaf, M. S. *J. Med. Chem.* **2006**, *49*, 23.
(22) Sonoda, M. T.; Martínez, L.; Webb, P.; Skaf, M. S.; Polikarpov, I. *Mol. Endocrinol.* **2008**, *22*, 1565.
(23) Carlsson, P.; Burendahl, S.; Nilsson, L. *Biophys. J.* **2006**, *9*, 3151.
(24) Martínez, L.; Polikarpov, I.; Skaf, M. S. *J. Phys. Chem. B* **2008**, *112*, 10741.
(25) Bleicher, L.; Aparicio, R.; Nunes, F. M.; Martínez, L.; Dias, S. M. G.; Figueira, A. C. M.; Santos, M. A. M.; Venturelli, W. H.; Silva, R.; Donate, P. M.; Neves, F. A. R.; Simeoni, L. A.; Baxter, J. D.; Webb, P.; Skaf, M. S.; Polikarpov, I. *BMC Struct. Biol.* **2008**, *8*, 8.
(26) Martínez, L.; Nascimento, A. S.; Nunes, F. M.; Phillips, K.; Aparicio, R.; Dias, S. M. G.; Figueira, A. C. M.; Lin, J. H.; Nguyen, P.; Apriletti, J. W.; Neves, F. A. R.; Baxter, J. D.; Webb, P.; Skaf, M. S.; Polikarpov, I. *Proc. Natl. Acad. Sci. U.S.A.* **2009**, *106*, 20717.
(27) Mayor, U.; Guydosh, N. R.; Johnson, C. M.; Grossmann, J. G.; Sato, S.; Jas, G. S.; Freund, S. M. V.; Alonso, D. O. V.; Daggett, V.; Fersht, A. R. *Nature* **2003**, *421*, 863.
(28) (a) Daggett, V. *Acc. Chem. Res.* **2002**, *35*, 422. (b) Daggett, V. *Chem. Rev.* **2006**, *106*, 1898.
(29) Li, A. J.; Daggett, V. *J. Mol. Biol.* **1996**, *257*, 412.
(30) Zhou, Y.; Karplus, M. *Nature* **1999**, *401*, 400.
(31) Agashe, V. R.; Shastry, M. C. R.; Udgaonkar, J. B. *Nature* **1995**, *377*, 754.
(32) Caflisch, A.; Karplus, M. *J. Mol. Biol.* **1995**, *252*, 672.
(33) Daggett, V.; Levitt, M. *J. Mol. Biol.* **1993**, *232*, 600.
(34) Snow, C. D.; Sorin, E. J.; Rhee, Y. M.; Pande, V. S. *Annu. Rev. Biomol. Struct.* **2005**, *34*, 43.
(35) Cavalli, A.; Ferrara, P.; Caflisch, A. *Proteins* **2002**, *47*, 305.
(36) Paliwal, A.; Asthagiri, D.; Bossev, D. P.; Paulaitis, M. E. *Biophys. J.* **2004**, *87*, 3479.
(37) Johansson, L.; Rudling, M.; Scanlan, T. S.; Lundasen, T.; Webb, P.; Baxter, J. D.; Angelin, B.; Parini, P. *Proc. Natl. Acad. Sci. U.S.A.* **2005**, *102*, 10297.
(38) Nunes, F. M.; Aparicio, M. A.; Santos, M. A. M.; Portugal, R. V.; Dias, S. M. G.; Neves, F. A. R.; Simeoni, L. A.; Baxter, J. D.; Webb, P.; Polikarpov, I. *Acta Crystallogr., Sect. D* **2004**, *10*, 1867.
(39) Greenfield, N.; Vijayanathan, V.; Thomas, T. J.; Gallo, M. A.; Thomas, T. *Biochem.* **2001**, *40*, 6646.
(40) Martínez, J. M.; Martínez, L. *J. Comput. Chem.* **2003**, *24*, 819.
(41) Martínez, L.; Andrade, R.; Birgin, E. G.; Martínez, J. M. *J. Comput. Chem.* **2009**, *77*, 2157.
(42) Phillips, J. C.; Braun, R.; Wang, W.; Gumbart, J.; Takhorshid, E.; Villa, E.; Chipot, C.; Skeel, R. D.; Kale, L.; Schulten, K. *J. Comput. Chem.* **2005**, *26*, 1781.
(43) MacKerell, A. D.; Bashford, D.; Bellott, M.; Dunbrack, R. L.; Evanseck, J. D.; Field, M. J.; Fischer, S.; Gao, J.; Guo, H.; Ha, S.; Joseph-McCarthy, D.; Kuchnir, L.; Kuczera, K.; Lau, F. T. K.; Mattos, C.; Michnick, S.; Ngo, T.; Nguyen, D. T.; Prodhom, B.; Reiher, W. E.; Roux, B.; Schlenkrich, M.; Smith, J. C.; Stote, R.; Straub, J.; Watanabe, M.; Wiorkiewicz-Kuczera, J.; Yin, D.; Karplus, M. *J. Phys. Chem. B* **1998**, *102*, 3586.
(44) Jorgensen, W. L.; Chandrasekhar, J.; Madura, J. D.; Impey, R. W.; Klein, M. L. *J. Chem. Phys.* **1983**, *79*, 926.
(45) Darden, T.; York, D.; Pedersen, L. *J. Chem. Phys.* **1993**, *98*, 10089.
(46) Heinig, M.; Frishman, D. *Nucl. Acid Res.* **1998**, *32* (Suppl. 2), W500–W502.
(47) Kearsley, S. K. *Acta Cryst. A* **1989**, *45*, 208.
(48) Holt, J. A.; Consler, T. G.; Williams, S. P.; Ayscue, A. H.; Leesnitzer, L. M.; Wisely, G. B.; Billin, A. N. *Mol. Endocrinol.* **2003**, *17*, 1704.
(49) Englander, S. W. *Annu. Rev. Biophys. Biomol. Struct.* **2000**, *29*, 213.
(50) McLaughlin, S. H.; Jackson, S. E. *Protein Sci.* **2002**, *11*, 1926.
(51) Nair, S. K.; Thomas, T. J.; Greenfield, N. J.; Chen, A.; He, H.; Thomas, T. *J. Mol. Endocrinol.* **2005**, *35*, 211.
(52) Gee, A. C.; Katzenellenbogen, J. A. *Mol. Endocrinol.* **2001**, *15*, 421.
(53) Sali, A.; Shakhnovich, E.; Karplus, M. *Nature* **1994**, *369*, 248.
(54) Onuchic, J. N.; Wolynes, P. G. *Curr. Opin. Struct. Biol.* **2004**, *14*, 70.
(55) Duan, Y.; Kollman, P. A. *Science* **1998**, *282*, 740.

JP911554P